Single gyroid in H-shaped block copolymers

So Jung Park [ORCID], Frank S. Bates [ORCID],[*] and Kevin D. Dorfman [ORCID][†]

Department of Chemical Engineering and Materials Science, University of Minnesota–Twin Cities, 421 Washington Ave. SE, Minneapolis, Minnesota 55455, USA

Single gyroid (SG) nanostructured materials, which consist of a single chiral network domain characterized by a triply periodic surface, are promising candidates for next-generation optical applications owing to a complete photonic band gap structure. However, due to thermodynamic metastability, accessing an equilibrium SG nanostructure through block copolymer self-assembly has been difficult to achieve experimentally. In contrast, the double gyroid (DG), consisting of two independent chiral networks, is a well-known stable phase in certain block copolymer systems. In this study, we predict an equilibrium SG phase formed in H-shaped $(BA)_2A(AB)_2$ block polymers, where two AB diblock arms are grafted onto each end of an A backbone. Using SCFT calculations, we constructed a phase diagram with respect to an architectural parameter α, defined as the volume fraction of an A backbone block to total A-type blocks, and the overall volume fraction of A blocks f_A. The SCFT phase diagram predicts an equilibrium SG stability window at $\alpha \approx 0.7$, and we confirm that the stability of SG extends to high segregation strength. Based on an analysis of the thermodynamic factors responsible for the relative stability of SG over DG, including free energy and geometric factors, we propose a molecular packing mechanism where the H-shaped polymers with asymmetric A blocks form a nearly constant mean curvature geometry of SG by localizing A/B junctions on the A/B interfaces and localizing the long A backbones in the majority domain to relieve the packing frustration. In contrast, the competitive DG phase suffers a considerable enthalpic penalty from the diffuse A/B interfaces created by inhomogeneous chain stretching to accommodate its larger mean curvature variation.

I. INTRODUCTION

Triply periodic minimal surface (TPMS) structures are characterized by three-dimensionally bicontinuous and triply periodic network domains divided by zero constant mean curvature (CMC) surfaces [1,2]. Owing to their unique geometric features, TPMS structures have attracted great attention for potential applications in photonics, metamaterials, separation membranes, and solar cells [3–10]. The most prevalent TPMS structures are topologically equivalent to the Schoen gyroid (G), Schwarz diamond (D), and Schwarz primitive (P) constructions, which consist of threefold, fourfold, and sixfold connected network channels divided by TPMSs, respectively. A common example observed in nature and artificial systems [11–13] is the double gyroid (DG, cubic $Ia\bar{3}d$ space symmetry), which contains two interpenetrating networks with opposite chirality, divided by a triply periodic matrix layer. DG is well known in block copolymer self-assembly system as an equilibrium phase situated between lamellar and cylindrical morphologies in phase diagrams, and it exhibits intermediate curvature between these two structures [14–18].

Each network substructure in the DG (with opposite chirality) is called a single gyroid (SG) when taken individually [19–24], and these SG cubic network domains have $I4_132$ space symmetry as the inversion symmetry of the DG is broken.

SG exhibits unique optical properties including a complete photonic band gap and inherent chirality, and it is found in nature as chiral photonic crystals. For example, the fascinating colors displayed by the butterfly *Callophrys rubi* are attributable to the SG structured chitin of the wing scales [19]. Owing to the exceptional optical properties predicted in SG structures, such as circular dichroism, negative light refraction, and a complete photonic band gap [3,25–29], many researchers have been inspired to artificially manufacture 3D SG crystals through top-down approaches such as nanoscale 3D printing [30,31], holographic lithography [32], or biotemplating of butterfly wing scales [19,29]. However, such top-down lithography is very challenging because precise unit-cell size is a prerequisite for optical applications ranging from subwavelength-scale metamaterials to optical crystals.

Block copolymer self-assembly is a versatile bottom-up process for designing various ordered mesoscale structures providing access to network structured materials with subwavelength-scale unit cells [16–18,33,34]. However, SG is known to be thermodynamically unstable in most block copolymer systems while DG is observed and predicted to be an equilibrium phase in experiment and theory, respectively [23]. For this reason, most attempts to target the SG

---

[*]bates001@umn.edu
[†]dorfman@umn.edu

nanostructure via block copolymer self-assembly have relied on deriving the SG from thermodynamically stable parent network structures. For example, the alternating gyroid phase, which forms in ABC triblock terpolymers and consists of two interpenetrating SG networks formed by A and C blocks, was used as a template to obtain an SG structure by selectively etching one of the networks and then backfilling with gold and removing the remaining polymer [20]. DG-forming block copolymers were also used for electroless plating to create SG-structured metallic nanoporous spheres [35]. As another strategy, Hsueh *et al.* demonstrated fabrication of an SG-like structure through heat treatment of the DG networks in PS/SiO_2 nanohybrids, which broke the inversion symmetry of the DG structure and resulted in a partially-opened bandgap [36]. In fact, there are some reports of SG inorganic scaffold formation in cooperative self-assembly of block polymers and silica precursors. Cao *et al.* reported interconversion between the SG and double diamond (DD) structure through the restricted epitaxial intergrowth in the cooperative self-assembly of a PEO-PS-PtBA triblock terpolymer and silica precursors [21]. An SG scaffold was also discovered during the structural transformation from the cylindrical to shifted DD phases in the self-assembly of diblock copolymer with silica precursors in solution [22].

However, an equilibrium SG phase self-assembled by block copolymers has never been reported experimentally. SG has been predicted to be thermodynamically metastable in most theories except for the BABAB pentablock copolymer [24], which is predicted by self-consistent field theory (SCFT) to form stable SG when the length ratio of the constituent blocks are appropriately tailored [24]. According to the SCFT study by Chen *et al.* on the origin of metastability of SG in AB diblock copolymers [23], the single gyroid phase is less stable than the DG phase because of the higher enthalpic energy per chain due to the higher interfacial area, which is caused by domain shrinking to compensate for the packing frustration of the AB diblock polymers in SG structure formation. It is considered that the packing frustration is high in the majority domain of SG [24], and thus far there is no established principle for guiding the design of block polymer architectures for equilibrium SG formation. For the purpose of achieving well-ordered SG nanostructures through block copolymer self-assembly, it is worth investigating unconventional, yet synthetically feasible, block copolymer architectures [37–39], and computational screening is a good starting point for this type of investigation.

In this study, we explore the SG phase in AB-type H-shaped block polymers, where four arms are grafted onto the ends of an A backbone block [see Fig. 1(a)]. This architecture is synthetically tractable [44], which makes understanding its potential for enabling useful phase behavior especially important. We tailored the polymer architecture by varying the architectural parameter α, defined as the volume fraction of the A backbone block to the total A-type blocks, ranging from an $(AB)_4$ star polymer ($\alpha = 0$), to a $(BA)_2A(AB)_2$ H-shaped polymer ($0 < \alpha < 1$), and progressively to a $(B)_2A(B)_2$ H-shaped polymer ($\alpha = 1$). We designed these H-shaped block polymers based on the hypothesis that if A is the majority block and B blocks form the struts, the A backbone of the H-shaped block polymer can relieve the packing frustration

in the majority domains of the SG phase provided the A backbone is sufficiently long. Also, we postulate that a highly asymmetric length of A arm blocks relative to the A backbone prevents the A/B interface from being highly curved into cylindrical or spherical phases, as demonstrated in $A(AB)_3$ miktoarm star copolymers where the interfacial curvature toward the minority B domain is suppressed by the inverted spontaneous curvature formed by the radial distribution of the short and long A blocks [45,46]. Furthermore, we anticipate the H architecture destabilizes the lamellar phase, which competes with network phases according to previous predictions [15,23], by frustrating the interdigitated packings in the lamellae, thereby opening a SG stability window between the cylindrical and lamellar phase windows. Inspired by this plausible mechanism for SG formation, we constructed the SCFT phase diagram with respect to α and the overall volume fraction of A blocks f_A by considering the 15 different candidate phases depicted in Fig. 1(b). We focus on the the B-rich side of the phase diagram where the stable SG formed by the B blocks exists in competition with DG and the orthorhombic single network O^{70} phases.

II. MOLECULAR MODELING AND METHOD

A. Self-consistent field theory

We used canonical ensemble SCFT [47–49] to investigate the equilibrium phase behavior of the H-shaped polymers in incompressible melts. The polymers are modeled as flexible Gaussian chains with N coarse-grained segments, where the statistical segment length of the A and B blocks is b. We consider an incompressible polymer melt consisting of n identical H-shaped polymers in a system volume V. In SCFT, the forward propagator $q(\mathbf{r}, s)$ and backward propagator $q^{\dagger}(\mathbf{r}, s)$ represent the complementary partial partition functions of a polymer chain, where s is a continuous coordinate parameter along the chain contour [47–49]. The partial fragment of polymer chain is specified by two ends, where one end is free and the other end, whose segment coordinate is s, is located at position $\mathbf{r}$. The forward and backward propagators are evaluated from the following modified diffusion equations:

$$\frac{\partial}{\partial s}q_{\tau}(\mathbf{r}, s) = \left(\frac{b^2}{6}\nabla^2 - \omega_{\gamma(s)}(\mathbf{r})\right)q_{\tau}(\mathbf{r}, s), \qquad (1)$$

$$-\frac{\partial}{\partial s}q_{\tau}^{\dagger}(\mathbf{r}, s) = \left(\frac{b^2}{6}\nabla^2 - \omega_{\gamma(s)}(\mathbf{r})\right)q_{\tau}^{\dagger}(\mathbf{r}, s), \qquad (2)$$

where $\omega_{\gamma(s)}$ represents the external chemical potential field acting on segment of type γ, which is either A or B depending on, in general, s for a given segment τ. The fields $\omega_{\gamma(s)}$ will be self-consistently determined by the mean-field equations, which are presented below.

The propagators are separately evaluated for the constituent blocks of the H-shaped polymer [see Fig. 1(a)], i.e., A backbone block ($\tau = A_b$), A arm block ($\tau = A_a$), and B arm block ($\tau = B$). The overall volume fraction of the four B blocks defines $f_B = 1 - f_A$, and the overall volume fraction of the A backbone block and the overall volume fraction of the four A arm blocks define $f_{A_b} = f_A\alpha$ and $f_{A_a} = f_A(1 - \alpha)$, respectively. The forward propagator and backward propagator for a B arm block starts from the free

(a)

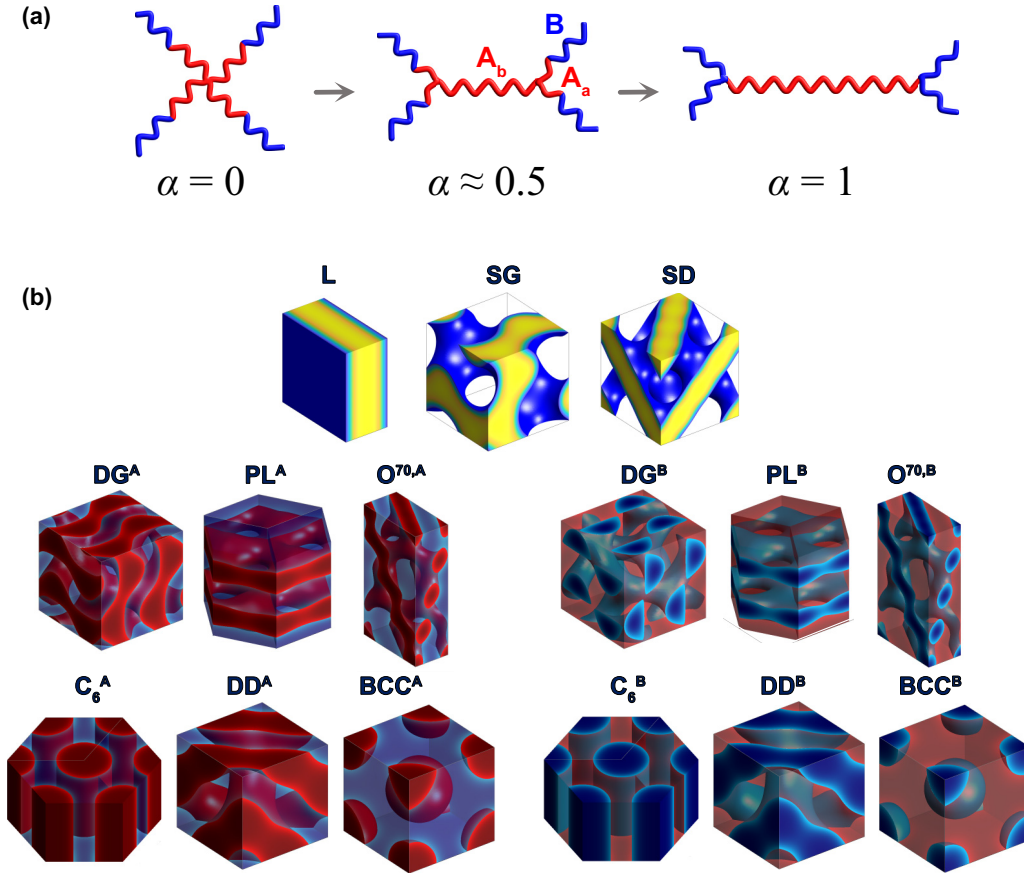$$\alpha = 0 \qquad \alpha \approx 0.5 \qquad \alpha = 1$$

(b)

FIG. 1. (a) Schematics of H-shaped AB block polymer architecture as function of α, defined as the volume fraction of the A_b backbone block to total A-type blocks including the A_a arm blocks. When $\alpha = 0$, the polymer architecture reduces to an $(AB)_4$ star copolymer, and when $\alpha = 1$, the polymer architecture reduces to a $(B)_2A(B)_2$ H-shaped polymer with B homopolymer arms. (b) Ordered candidate phases for the SCFT calculations. For lamellae (L), single gyroid (SG), single diamond (SD), the minority and majority domains on the A-rich and B-rich sides of the phase diagram are related by an inversion symmetry. Double gyroid (DG^A), perforated lamellae (PL^A), *Fddd* ($O^{70,A}$), hexagonal-packed cylinders (C_6^A), double diamond (DD^A), and body-centered cubic spheres (BCC^A) have A (red) domain structures in the matrix of B (blue) domains, and DG^B, PL^B, $O^{70,B}$, C_6^B, DD^B, and BCC^B have B (blue) domain structures in the matrix of A (red) domains. The space group symmetry for each structure is provided in the Supplemental Material (SM) [40].

end ($s = 0$) and the AB junction ($s = Nf_B/4$) with initial conditions $q_B(\mathbf{r}, 0) = 1$ and $q_B^\dagger(\mathbf{r}, Nf_B/4) = q_{A_a}^\dagger(\mathbf{r}, 0)$, respectively. The forward propagator and backward propagator for an A arm block starts from the AB junction ($s = 0$) and the AA junction ($s = Nf_{A_a}/4$) with initial conditions $q_{A_a}(\mathbf{r}, 0) = q_B(\mathbf{r}, Nf_B/4)$ and $q_{A_a}^\dagger(\mathbf{r}, Nf_{A_a}/4) = q_{A_b}^\dagger(\mathbf{r}, 0)q_{A_a}(\mathbf{r}, Nf_{A_a}/4)$, respectively. Lastly, the forward propagator and backward propagator for the A backbone starts from one of the AA junctions ($s = 0$) and the other AA junction ($s = Nf_{A_b}$), respectively, with initial conditions $q_{A_b}(\mathbf{r}, 0) = q_{A_b}^\dagger(\mathbf{r}, Nf_{A_b}) = [q_{A_a}(\mathbf{r}, Nf_{A_a}/4)]^2$.

From the computed propagators, the segment densities $\phi_\gamma(\mathbf{r})$ of segment type γ in units of inverse segment volume are determined by

$$\phi_A(\mathbf{r}) = \frac{1}{NQ}\left[4\int_0^{Nf_{A_a}/4} ds\, q_{A_a}(\mathbf{r}, s)q_{A_a}^\dagger(\mathbf{r}, s)\right.$$

$$\left. + \int_0^{Nf_{A_b}} ds\, q_{A_b}(\mathbf{r}, s)q_{A_b}^\dagger(\mathbf{r}, s)\right], \qquad (3)$$

$$\phi_B(\mathbf{r}) = \frac{4}{NQ}\int_0^{Nf_B/4} ds\, q_B(\mathbf{r}, s)q_B^\dagger(\mathbf{r}, s), \qquad (4)$$

where Q is the total partition function of the H-shaped polymer,

$$Q = \frac{1}{V}\int d\mathbf{r}\, q_\tau(\mathbf{r}, s)q_\tau^\dagger(\mathbf{r}, s). \qquad (5)$$

Equation (5) is a generic expression of total partition function with an arbitrary choice of τ and s. If s is chosen to be at a junction in the H-shaped polymer, the evaluation of the total partition function takes into account the joint probability distribution. For example, in the software we used to solve the mean-field equations, s is chosen at one of the AA junctions. Therefore, the total partition function was evaluated by

$$Q = \frac{1}{V}\int d\mathbf{r}\, q_{A_b}(\mathbf{r}, 0)q_{A_b}^\dagger(\mathbf{r}, 0) \qquad (6)$$

where $q_{A_b}(\mathbf{r}, 0) = [q_{A_a}(\mathbf{r}, Nf_{A_a}/4)]^2$ takes into account the joint probability distribution from the two arms grafted onto the backbone.

In the mean-field approximation, the solutions for the densities and chemical potential fields satisfy the following self-consistent mean field equations:

$$\omega_A(\mathbf{r}) = \chi\phi_B(\mathbf{r}) + \xi(\mathbf{r}), \tag{7}$$

$$\omega_B(\mathbf{r}) = \chi\phi_A(\mathbf{r}) + \xi(\mathbf{r}), \tag{8}$$

where χ is the Flory-Huggins interaction parameter for interaction between A and B segments, and ξ is the pressure field enforcing the incompressiblity constraint, $\phi_A(\mathbf{r}) + \phi_B(\mathbf{r}) = 1$. The Helmholtz free energy per H-shaped polymer chain is calculated from the self-consistent mean-field solutions as

$$\frac{F}{nk_BT} = -\ln(eQ) + \frac{\chi N}{V}\int d\mathbf{r}\,\phi_A(\mathbf{r})\phi_B(\mathbf{r})$$
$$- \frac{N}{V}\int d\mathbf{r}[\omega_A(\mathbf{r})\phi_A(\mathbf{r}) + \omega_B(\mathbf{r})\phi_B(\mathbf{r})] \tag{9}$$

where k_B is the Boltzmann factor and T is the system temperature.

We solved the nonlinear self-consistent mean-field equations using the open-source C + + software package Polymer Self-Consistent Field (PSCF) developed by Morse and coworkers [49,50]. By comparing the free energies of 15 competitive candidate phases [Fig. 1(b)], the equilibrium phase is identified at a given system parameter and the full phase diagrams are constructed. The details of the SCFT simulation method and the candidate phases are provided in Sec. S1 of the Supplemental Material (SM) [40].

B. Free-energy decomposition

Free-energy analysis is usually done by decomposing the Helmholtz free energy into separate free-energy contributions, for example, enthalpic free energy and entropic free energy. In SCFT, it is straightforward to compute the separate free energy terms from the established SCFT formulations once the converged SCFT solutions are determined. Because of this simplicity, SCFT free-energy analysis is often adopted as a strategy to dissect phase behavior in various types of block copolymers [23,45,51]. The Helmholtz free-energy expressions in Eq. (9) can be decomposed into the enthalpic contribution, which represents the interaction energy penalty for the unfavorable contacts between the A/B monomers, and the entropic contribution, which represents the free-energy penalty from the entropy loss associated with chain stretching or compression along with localization of the block copolymer at the domain interface. The free energy is expressed as

$$\frac{F}{nk_BT} = \frac{U}{nk_BT} - \frac{S}{nk_B} - 1 \tag{10}$$

where U is the internal energy and S is total entropy of the system. Here, the last term does not have any physical meaning but serves as a convenient reference state for the Helmholtz

free energy. The internal energy U and the total entropy S are calculated by

$$\frac{U}{nk_BT} = \frac{\chi N}{V}\int d\mathbf{r}\,\phi_A(\mathbf{r})\phi_B(\mathbf{r}) \tag{11}$$

$$-\frac{S}{nk_B} = -\ln Q - \frac{N}{V}\int d\mathbf{r}[w_A(\mathbf{r})\phi_A(\mathbf{r}) + w_B(\mathbf{r})\phi_B(\mathbf{r})] \tag{12}$$

In this study, the entropic contribution $-S/nk_B$ is further decomposed into the contribution from the translational entropy of different type of junctions in the H-shaped polymer architecture, and the contribution from the configurational entropy of the blocks, where loss comes from chain stretching of each block. The SCFT formulations for the separate entropy contributions are provided in Sec. S2 of the SM [40].

C. Geometric analysis method

For the geometric analysis of the SG and DG structures, we performed mean curvature and interfacial area calculations using a slightly modified version of the software originally developed by Feng *et al.* [52] and modified by Chen *et al.* [23]. In this analysis, the A/B domain interface is identified by constructing a triangulated mesh from a linear interpolation of the converged SCFT density fields to identify the locations where $\phi_A(\mathbf{r}) = \phi_B(\mathbf{r}) = 0.5$. The mean curvature $H = (\kappa_1 + \kappa_2)/2$ is obtained by computing the principal curvatures κ_1 and κ_2 on each triangulated vertex, with a sign convention that principle curvature is positive when the interface is curved towards the B domain. Interfacial area is readily computed by summing the area of each triangle in the mesh, and it is divided by the volume of the unit cell to compare the interfacial area per unit volume of the SG and DG phases.

III. RESULTS AND DISCUSSION

A. Phase diagrams

To investigate the effects of molecular architecture on the phase behavior of the H-shaped polymer, we constructed the phase diagram with respect to α and volume fraction of A blocks f_A at fixed $\chi N = 60$ as shown in Fig. 2. As noted at the outset, we will focus on the B-rich side of the phase diagram. When $\alpha = 0$, we obtain the conventional phase sequence $C_6^A \to DG^A \to L \to DG^B \to C_6^B \to BCC^B$ with increasing f_A [53]. As α increases from 0 to 1, the phase boundaries shift nonmonotonically. Consequently, around $\alpha = 0.7$, there is a wide DG^A phase region with $\Delta f_A^{DG^A} \approx 0.11$ and relatively narrow lamellar phase region with $\Delta f_A^L \approx 0.10$, when compared to those observed in the conventional linear AB diblock copolymer phase diagram, where $\Delta f_A^{DG^A} = 0.02$ to 0.03 and $\Delta f_A^L > 0.2$ at high segregation strength [54]. The same phase boundary shifts on the A-rich side were observed in the SCFT phase diagrams of $A(AB)_n$ miktoarm star copolymers calculated by Li *et al.* [45], where the miktoarm star copolymer model with $n = 2$ can be regarded as a decomposed unit of our H-shaped polymers [53]. They attributed the significantly widened DG^A stability window to the large deflection of the G/L boundary, which was caused by synergetically relieved packing frustrations in DG; the long A arms relieve the packing frustration at
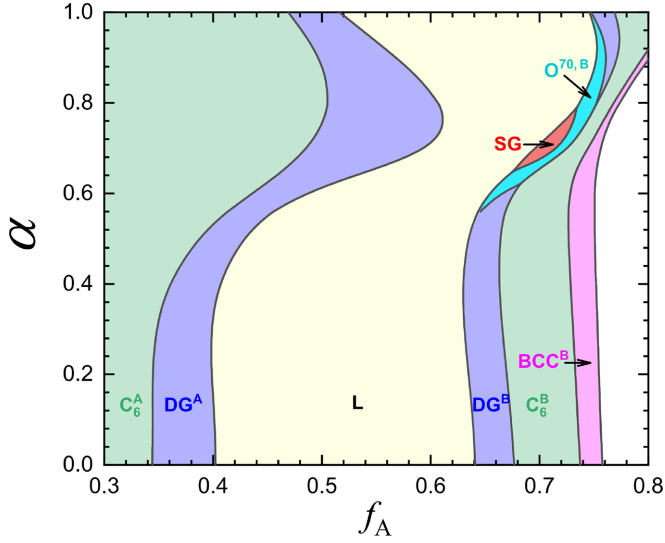
FIG. 2. Equilibrium phase diagram of H-shaped block polymers with respect to architectural parameter α and overall volume fraction of A block f_A at fixed $\chi N = 60$. The stability windows of the ordered phases are colored, and the white empty region corresponds to the homogeneous disordered state. Free-energy data for each phase are provided in Fig. S1 within the SM [40]. The resolved points for the phase boundary construction are provided in Fig. S8 within the SM [40].

FIG. 3. Equilibrium phase diagram of H-shaped block polymers with respect to interaction parameter χN and f_A, at fixed $\alpha = 0.7$. Free-energy data for each phase are provided in Fig. S2 within the SM [40]. The resolved points for the phase boundary construction are provided in Fig. S9 within the SM [40].

the centers of the gyroid nodes, and the short A blocks of the diblock arms smear the A/B interface to relax the high packing frustration near the saddle surface.

The phase diagram of the H-shaped polymer in Fig. 2 exhibits interesting behaviors on the B-rich side ($f_A > 0.5$). Around $\alpha = 0.7$, the DG^B window region disappears and is replaced by emergence of stable regions of the SG and $O^{70,B}$ phases; both phases are single network structures. The free-energy comparison in the SG stability region at $\alpha = 0.7$ (see Fig. S1(b) within the SM [40]) confirms that SG is the most stable phase among the candidate phases with the free energy difference $\Delta F/nk_B T \approx 0.005$ with respect to the next-lowest free-energy phases (L or $O^{70,B}$). Emergence of the SG stability window near $\alpha \approx 0.7$, where the L window width is minimized, supports the previous arguments that SG is less unstable along the DG/L boundary, and thus destabilizing the L phase is favorable to formation of SG [23]. At the specific parameter values, $f_A = 0.7$ and $\alpha = 0.7$, where SG is stable, the length of the constituent blocks in the H-shaped polymer architecture are $N_{A_b} = 0.49N$, $N_{A_a} = 0.053N$, and $N_B = 0.075N$, where N is the total degree of polymerization.

To investigate the robustness of the SG stability in the H-shaped polymers, we constructed a phase diagram with respect to χN and f_A, at fixed $\alpha = 0.7$ (Fig. 3). The resulting phase diagram shows that the SG stability window extends to high segregation strength, while the $O^{70,B}$ stability window only exists at relatively low segregation strength, which is a generally observed feature in AB-type block polymer phase diagrams [53]. The minimum χN for an order-disorder transition (ODT) is expected to be located below $\chi N = 30$. Also noteworthy is that DG^B is metastable throughout the depicted range of the phase diagram; SG replaces DG^B in the
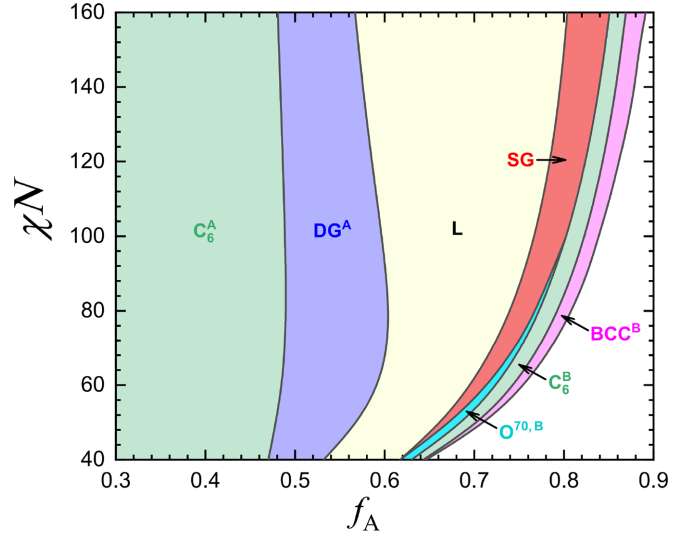
conventional phase sequence ($C_6^A \rightarrow DG^A \rightarrow L \rightarrow DG^B \rightarrow C_6^B$) at high segregation strength. Considering the position of the SG stability window in the phase sequence and the analogous morphologies of the SG and DG phases, we speculate that the width of SG stability window will be limited by the nearly vertical slope of the phase boundaries in the strong segregation limit, similar to the prediction for the DG window in linear AB diblock copolymers [54].

B. Free-energy and geometric analysis

In this subsection, we provide a free-energy analysis to identify the factors responsible for the relative stability of SG over DG and examine the A/B interface geometry to model the molecular self-assembly mechanisms in H-shaped block polymers, as discussed in the following subsection.

In Fig. 4, the Helmholtz free-energy difference $F_{SG} - F_{DG^B}$ between SG and DG^B is decomposed into the enthapic parts and the entropic parts at $\chi N = 60$ and $\alpha = 0.7$. Within the range of f_A where SG is predicted to be stable ($0.696 < f_A < 0.715$), the free-energy decomposition indicates that the enthalpic contribution affects the free-energy difference more strongly than the entropic contribution, which leads to the negative values of $F_{SG} - F_{DG^B}$ within the SG stability window as a result of competition between the enthapic penalty and the entropy loss. This result is interpreted as DG^B being less stable than SG due to the higher enthalpic energy per polymer chain. This is opposite to the prior SCFT free-energy analysis on the linear AB diblock copolymers from Chen *et al.* [23], where SG is less stable than DG due to the higher enthalpic energy per polymer. The reason for this discrepancy is a difference in the molecular packing mechanisms between SG and DG^B for the linear diblock copolymers to relieve the packing frustrations when compared to what we will describe shortly for the H polymers. For the linear diblock copolymers, in
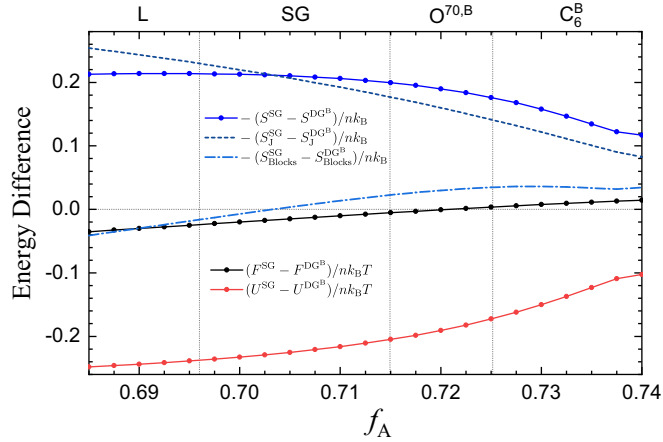
FIG. 4. Decomposition of Helmholtz free-energy differences between the SG and DG$^\mathrm{B}$ phases at $\chi N = 60$ and $\alpha = 0.7$. The black line represents the difference of Helmholtz free energy per H-shaped polymer $(F^{\mathrm{SG}} - F^{\mathrm{DG}^\mathrm{B}})/nk_\mathrm{B}T$, and the blue line represents the entropic contribution $-(S^{\mathrm{SG}} - S^{\mathrm{DG}^\mathrm{B}})/nk_\mathrm{B}$, and the red line represents the enthalpic contribution $(U^{\mathrm{SG}} - U^{\mathrm{DG}^\mathrm{B}})/nk_\mathrm{B}T$. The dark blue dashed line corresponds to the translational entropic energy of total junctions (A/A and A/B junctions), and the light blue dash-dotted line corresponds to the configurational entropic energy of the total blocks in the H-shaped polymer architecture. The vertical dotted lines denote the boundaries of the stability windows for the L, SG, O$^{70,\mathrm{B}}$, and C$^\mathrm{B}_6$ phases over the range of f_A.

order to maintain the nearly constant mean curvature structure of SG and simultaneously reduce total chain stretching penalties, SG tends to shrink its domain sizes, which leads to the larger interfacial areas per unit volume than that of DG. The higher enthalpic penalty per linear diblock polymer chain is due to the larger interfacial area per unit volume in the SG phase, which is the major cause of the metastability of SG in the linear diblock copolymer melts.

In Fig. 4, we further decompose the entropic free energy into the contribution from the translational entropy loss of junctions in the H-shaped polymer architecture and the contribution from the configurational entropy loss of the polymer blocks, which represents the stretching free energy. The data show that the difference in the entropic contribution is mainly from the translational entropy loss of the junctions rather than the configurational entropy loss of the polymer blocks, and the loss of translational entropy of junctions comes more from the A/B junctions than the AA junctions, which is due to the tendency to localize A/B junctions (Fig. S3 within the SM [40]) between A and B domains. The higher loss of translational entropy of A/B junctions in SG than in DG$^\mathrm{B}$ can be explained by the less homogeneously distributed A/B interfaces per unit cell of the SG phase than that of the DG$^\mathrm{B}$ phase.

While the results of this free-energy analysis led to opposite conclusions between the linear diblock polymer [23] and the H-shaped polymer, the network structures formed by the both architectures exhibit similar distributions in mean curvature H, as we would expect if the A/B interfaces are relatively sharp. Figure 5 shows the mean curvature maps on the A/B interface defined by $\phi_\mathrm{A} = \phi_\mathrm{B} = 0.5$ for the network structures in the SG and DG$^\mathrm{B}$ phases, respectively. SG has
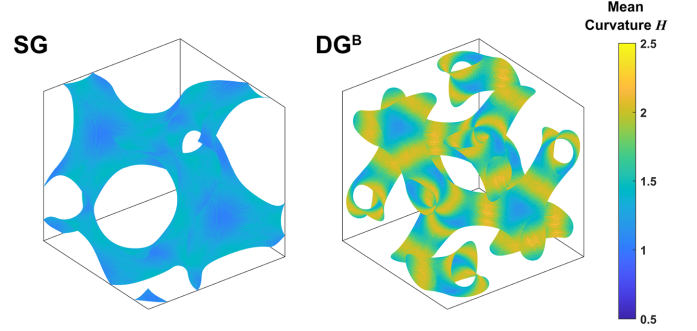

FIG. 5. Mean curvature maps over the A/B interfaces of the SG (left) and the DG$^\mathrm{B}$ structures (right) formed by the H-shaped polymers at $\alpha = 0.7$, $\chi N = 60$, and $f_\mathrm{A} = 0.7$. The mean curvatures H are scaled by $1/a\sqrt{N}$.

nearly constant mean curvature with relatively low average mean curvature, while the DG$^\mathrm{B}$ exhibits large deviation from the constant mean curvature geometry, noticeably on the interfacial regions of the threefold connecting nodes, similar to the curvature map of the linear diblock copolymer [15]. The [111] direction views of the same curvature maps are provided in Fig. S4 within the SM [40]. According to the mean curvature histograms in Fig. S5 within the SM [40], DG$^\mathrm{B}$ has a higher standard deviation in mean curvature and higher average mean curvature ($\sigma_H = 0.264/aN^{1/2}$, $\langle H \rangle = 1.701/aN^{1/2}$) than those of SG ($\sigma_H = 0.106/aN^{1/2}$, $\langle H \rangle = 1.281/aN^{1/2}$). Furthermore, as in the case of the linear diblock copolymers [23], the interfacial area per unit-cell volume of SG ($A/V = 2.11/aN^{1/2}$) is larger than that of DG$^\mathrm{B}$ ($A/V = 2.01/aN^{1/2}$), which is due to the decreased domain size of SG (Fig. S6 within the SM [40]). These results suggest that, similar to the linear diblock copolymers, H-shaped polymers also tend to reduce the domain sizes of SG to relieve the packing frustration while maintaining a nearly constant mean curvature geometry, whereas DG$^\mathrm{B}$ stretches the polymer chains inhomogeneously to relieve high packing frustration at the center of the threefold nodes and to accommodate the large deviation from constant mean curvature geometry.

However, the larger enthalpic energy per polymer in DG$^\mathrm{B}$ than SG (Fig. 4) (but a smaller interfacial area per polymer, which is proportional to A/V) implies that the degree of mixing between A and B monomers in the interfacial regions, where the unfavorable A and B contacts occur, should be much different between SG and DG$^\mathrm{B}$. The enthalpic energy is related to the interfacial energy from the unfavorable A/B monomer contacts, which is proportional to $\int w_\mathrm{I} dA$, where w_I is the effective interfacial width, a measure of how the density profile of A(B) type monomers changes from A(B) majority to B(A) majority. Therefore, the effective interfacial width in the DG$^\mathrm{B}$ phase should be greater than for SG in order to account for the larger interfacial energy in the former given the smaller interfacial area per polymer. We believe that even at the same segregation strength χN, the overall interfacial density profiles in the DG$^\mathrm{B}$ and SG phases are not the same given how the H-shaped polymers self-assemble and form the interfaces, leading to a broader interfacial width in the DG$^\mathrm{B}$ versus the SG phase.
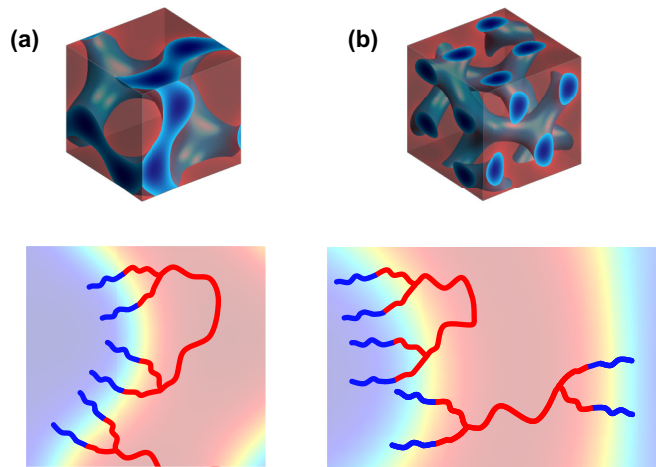
FIG. 6. Depictions of H-shaped polymer chain configurations forming A/B interfaces in (a) SG and (b) DG^B phases.

C. Molecular packing mechanism

Based on the analysis in Sec. III B, we propose that the H-shaped polymers adopt two different molecular configurations when self-assembling into the SG and DG^B phases. In the SG phase, most of the packing frustration exists in the majority domains while for the DG phase, packing frustration is high at the center of the bulky network nodes [15,24]. The H-shaped polymer architecture parameters that form the stable SG phase in our study have relatively symmetric A/B block compositions in the AB diblock arms compared to the highly asymmetric lengths between the A backbone and the A arm blocks. Figure 6(a) depicts a model of the resulting chain configurations in the SG phase. In order to reduce the total stretching penalty, the unit-cell size shrinks to accommodate the network domains with the relatively short B blocks. Through locating the AB junctions of the diblock arms on the interfaces, the relatively symmetric diblock arms form the low interfacial curvatures of the SG structure with the long A backbones stretched to relieve the packing frustration in the majority domains through the core-shell distributions of the long and short asymmetric A blocks. Since the SG structure tends to adopt a nearly constant mean curvature geometry (Fig. 5), the interfacial width and AB junction distributions within the interfaces would not vary considerably over the interfacial surface. On the other hand, for the DG^B phase in Fig. 6(b), we expect that the AB junctions are less localized within the diffuse interfaces to accommodate the large curvature variation in the DG^B phase shown in Fig. 5. At the expense of a small amount of A/B interfacial energy from the diffuse interfaces, the H-shaped polymers reduce the packing frustration associated with forming the bulky threefold connecting nodes, characterized by large deviation from the constant mean curvature, by inhomogeneously stretching the chains. The more delocalized A/B junctions within the diffuse A/B interface of the DG^B phase can also account for the lower translational entropy loss of the A/B junctions, evidenced by the lower translational entropy contribution to the free energy in Fig. S3 within the SM [40].

For the three-dimensional morphologies, it is difficult to compare the segmental density profiles at the interfaces be-

tween different phases by examining only one direction along the unit cell. Furthermore, the domain shape, mean curvature, and normal vector of the interfaces are significantly different along different directions, so the density profile along the same direction cannot be taken as equivalent for the comparison between the different phases. For our best approximation, we choose the [111] direction for comparison between the SG and DG^B phases, which passes through the centers of four threefold connectors of the DG^B per unit cell and the centers of two threefold connectors of the SG per unit cell, thus providing a rational basis for comparison. The mean curvatures of the interfaces along the [111] direction are relatively low compared to the average $\langle H \rangle$ for both SG and DG^B ($H < 1.25$), and the interfacial normal vector is considered to be nearly parallel to the [111] direction [1,2,25] (see Fig. S10 within the SM [40]).

Figure 7 presents the volume fraction profiles of each block and the spatial distributions of each junction along the [111] direction in each unit cell. As shown in Figs. 7(a) and 7(b), the A arm blocks are mostly distributed between the A and B domains for both SG and DG^B phases. In both cases, there is a small amount of A arm block mixed at the center of the B domains, which implies there exists a small percentage of the polymer configurations where the short arms of the H-shaped polymers are excessively stretched to fill the center of the B domains. At the centers of the A domains, there is 89% volume fraction of A backbone blocks for the SG phase, while there is 75% volume fraction of A backbone blocks for the DG^B phase. For the SG phase, the network domains (B domains) are less homogeneously distributed in the unit cell, so the A backbones have to be more stretched to fill the center of the thick majority domain (A domains) than in the DG^B phase. In Figs. 7(c) and 7(d), the concentrations of both A/A and A/B junctions of the H-shaped polymer at the center of the A domains are lower in SG than in DG^B, which supports a hypothesis that the center of the A domains are filled mostly by the A backbone in the SG phase. This result suggests that the H-polymer architecture with its long backbone is favorable to relieve the high packing frustration in the majority domain of the SG morphology. The analogous data for the [101] direction (Fig. S7 within the SM [40]) also shows the distribution profiles, again consistent with the chain packing schematic in Fig. 6.

From the density profiles in Figs. 7(a) and 7(b), we compute the approximate interfacial width w_I where the density profile switches from the A(B) majority domain to the B(A) majority domain [47], i.e., $w_I \equiv (\phi_B^{max} - \phi_B^{min})/|\phi_B'|$, where ϕ_B^{max} and ϕ_B^{min} are the maximum and minimum values of ϕ_B at the centers of the B and A domains, respectively, and ϕ_B' is the slope of the density profile at the position **r**, where $\phi_B(\mathbf{r}) = 0.5$. The interfacial width obtained from the density profiles along the [111] direction are very similar between the SG and the DG^B ($w_I/aN^{1/2} = 0.111$ for the SG and $w_I/aN^{1/2} = 0.114$ for the DG^B). The relatively thin interfacial widths suggest that the mean curvatures (Fig. 5) are more affected by situating the matrix forming block termini along the TPMS like surface [13] rather than the interfacial density profiles. However, as mentioned earlier, there is a shortcoming to comparing the interfacial width based on the this method due to the different morphologies and mean curvatures. Considering the
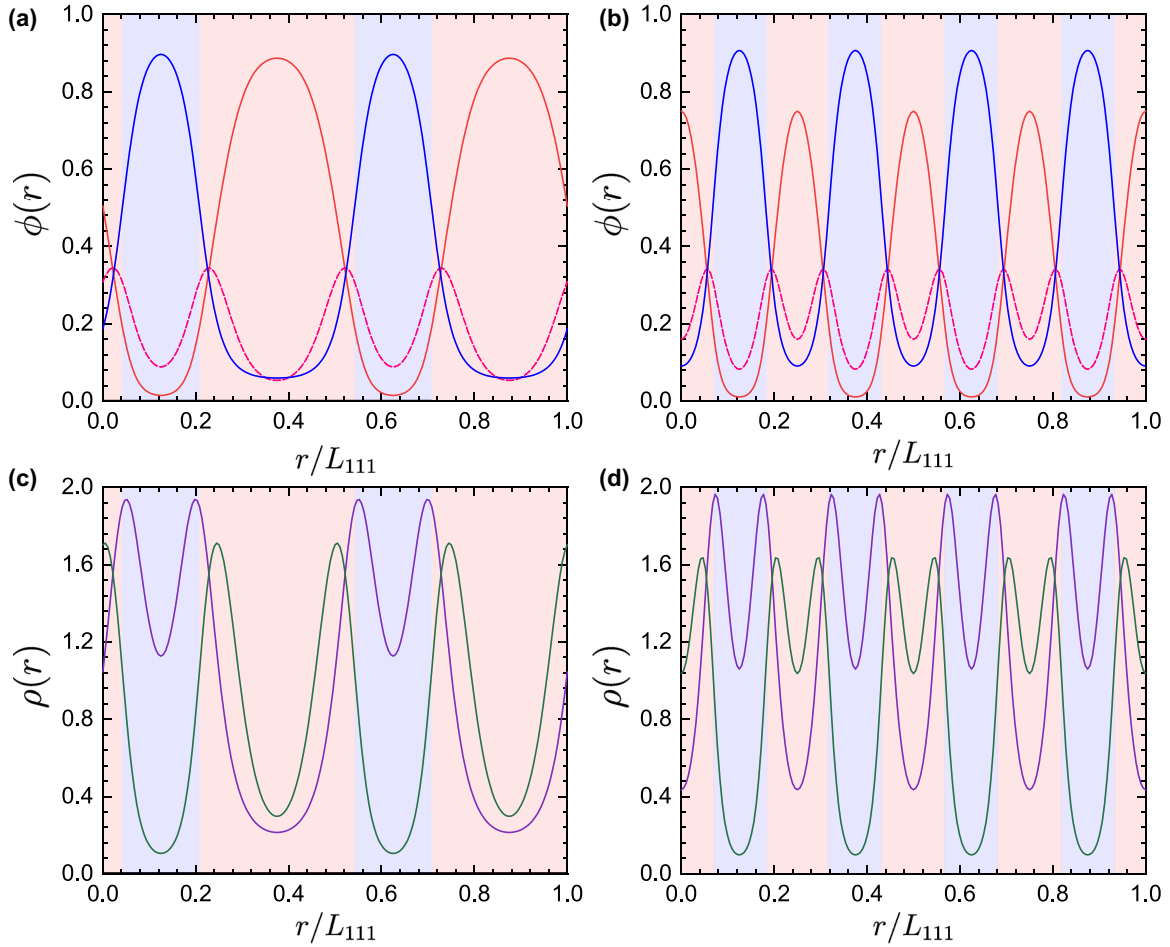
FIG. 7. [(a),(b)] Density profiles for the B blocks (blue lines), A_b backbone blocks (red lines), A_a arm blocks (pink dashed lines) along the [111] direction of unit cells for (a) SG and (b) DG^B phases formed by H-shaped polymers at $\alpha = 0.7$, $\chi N = 60$, and $f_A = 0.7$. [(c),(d)] The positional probability densities of single A/A junction (purple lines) and single A/B junction (green lines) in the same unit cells for (c) SG and (d) DG^B phases.

higher interaction free energy and the lower interfacial area per unit volume for DG^B than SG, as discussed in Sec. III B, it is obvious that the overall interfacial width in DG^B, averaged over the surface with every interfacial normal vector accounted for, should be broader than that of SG. We propose that the different chain packing mechanisms of the H-shaped polymer architectures for relieving the packing frustrations in the SG and the DG^B phases illustrated in Fig. 6 induce the different interfacial density profiles, leading to the different interfacial energy per chain, which results in the more stable SG phase with the lower Helmholtz free energy than the metastable DG^B phase in the H-shaped polymers.

One open question is the impact of polydispersity on the stability of SG in H-shaped polymers. We anticipate that polydispersity will be a stabilizing effect because the challenge in realizing network phase formation is relieving packing frustration [15], which can be done through localization of polymers with different degrees of polymerization [55]. Importantly, polydispersity would tend to destabilize the competing lamellar phase owing to nonuniform chain stretching. A definitive test of this hypothesis in the context of H-shaped polymers would require additional SCFT calculations, along the lines of what has been done for

double diamond and plumber's nightmare phases in binary blends [55], and represents an interesting line of further research.

IV. CONCLUSIONS

In summary, we investigated the phase behavior of H-shaped $(BA)_2A(AB)_2$ block polymers by constructing phase diagrams using SCFT calculations. A stable SG phase window is predicted between L and $O^{70,B}$ phase regions. When the size of the A arm block relative to the A backbone block is modestly asymmetric (e.g., $\alpha \approx 0.7$), the phase diagram exhibits skewed phase boundaries toward the B-rich side, expanding the phase regions for the A structures, due to the conformational asymmetry arising from the architectural asymmetry between A and B blocks. However, when increasing f_A further, an equilibrium SG phase is predicted next to the asymmetric lamellar phase on the phase diagram of the H-shaped polymers (Figs. 2 and 3). We speculate destabilization of asymmetric lamellar phase by molecular packing frustration contributes to the emergence of the SG phase, which has relatively low interfacial curvature with more CMC-like structure than DG. It is noticeable that the next competitive

phases to the SG phase in terms of free energy were usually L, $O^{70,B}$, and PL^B phases, rather than the DG^B phase.

Based on this speculation, we suggest that destabilizing interdigitated packing in the lamellar phase by molecular architecture and reducing packing frustration in the majority domain by asymmetric blocks is a good strategy to promote single network phases, and it can be achieved using a dendrimer-like polymer [39], or an H-shaped polymer with an asymmetric number of arms. The SCFT predictions presented here indicate that an SG phase is accessible, and identified a region of the state space for future experimental work. The synthetic approaches for these type of architectures are accessible through stepwise iterative methodologies using living anionic polymerization [37–39], and a synthetic strategy for this architecture has been recently presented [44]. In conclusion, accessing an equilibrium SG morphology through tailored H-shaped polymer architectures should be feasible using recently developed synthetic methods. The resulting single network structure is promising for creating advanced optical materials with a complete photonic band gap.

[1] A. H. Schoen, Infinite periodic minimal surfaces without self-intersections, NASA Technical Report No. D-5541 (1970), https://ntrs.nasa.gov/citations/19700020472.

[2] M. Wohlgemuth, N. Yufa, J. Hoffman, and E. L. Thomas, Triply periodic bicontinuous cubic microdomain morphologies by symmetries, Macromolecules **34**, 6083 (2001).

[3] J. A. Dolan, B. D. Wilts, S. Vignolini, J. J. Baumberg, U. Steiner, and T. D. Wilkinson, Optical properties of gyroid structured materials: From photonic crystals to metamaterials, Adv. Opt. Mater. **3**, 12 (2015).

[4] J. A. Dolan, M. Saba, R. Dehmel, I. Gunkel, Y. Gu, U. Wiesner, O. Hess, T. D. Wilkinson, J. J. Baumberg, U. Steiner, and B. D. Wilts, Gyroid optical metamaterials: Calculating the effective permittivity of multidomain samples, ACS Photonics **3**, 1888 (2016).

[5] A. M. Urbas, M. Maldovan, P. DeRege, and E. L. Thomas, Bicontinuous cubic block copolymer photonic crystals, Adv. Mater. **14**, 1850 (2002).

[6] M. Stefik, S. Guldin, S. Vignolini, U. Wiesner, and U. Steiner, Block copolymer self-assembly for nanophotonics, Chem. Soc. Rev. **44**, 5076 (2015).

[7] D. L. Gin, J. E. Bara, R. D. Noble, and B. J. Elliott, Polymerized lyotropic liquid crystal assemblies for membrane applications, Macromol. Rapid Commun. **29**, 367 (2008).

[8] L. Li, L. Schulte, L. D. Clausen, K. M. Hansen, G. E. Jonsson, and S. Ndoni, Gyroid nanoporous membranes with tunable permeability, ACS Nano **5**, 7754 (2011).

[9] E. J. Crossland, M. Kamperman, M. Nedelcu, C. Ducati, U. Wiesner, D. M. Smilgies, G. E. Toombes, M. A. Hillmyer, S. Ludwigs, U. Steiner, and H. J. Snaith, A bicontinuous double gyroid hybrid solar cell, Nano Lett. **9**, 2807 (2009).

[10] P. Docampo, M. Stefik, S. Guldin, R. Gunning, N. A. Yufa, N. Cai, P. Wang, U. Steiner, U. Wiesner, and H. J. Snaith, Triblock-terpolymer-directed self-assembly of mesoporous TiO_2: High-performance photoanodes for solid-state dye-sensitized solar cells, Adv. Energy Mater. **2**, 676 (2012).

[11] S. Andersson, S. T. Hyde, K. Larsson, and S. Lidin, Minimal surfaces and structures: From inorganic and metal crystals to cell membranes and biopolymers, Chem. Rev. **88**, 221 (1988).

[12] V. Saranathan, A. E. Seago, A. Sandy, S. Narayanan, S. G. Mochrie, E. R. Dufresne, H. Cao, C. O. Osuji, and R. O. Prum, Structural diversity of arthropod biophotonic nanostructures spans amphiphilic phase-space, Nano Lett. **15**, 3735 (2015).

[13] T. Oka, N. Ohta, and S. T. Hyde, Polar-nonpolar interfaces of normal bicontinuous cubic phases in nonionic surfactant/water systems are parallel to the gyroid surface, Langmuir **36**, 8687 (2020).

[14] D. A. Hajduk, P. E. Harper, S. M. Gruner, C. C. Honeker, G. Kim, L. J. Fetters, and G. Kim, The gyroid: A new equilibrium morphology in weakly segregated diblock copolymers, Macromolecules **27**, 4063 (1994).

[15] M. W. Matsen and F. S. Bates, Origins of complex self-assembly in block copolymers, Macromolecules **29**, 7641 (1996).

[16] F. S. Bates, Network phases in block copolymer melts, MRS Bull. **30**, 525 (2005).

[17] A. J. Meuler, M. A. Hillmyer, and F. S. Bates, Ordered network mesostructures in block polymer materials, Macromolecules **42**, 7221 (2009).

[18] X. B. Wang, T. Y. Lo, H. Y. Hsueh, and R. M. Ho, Double and single network phases in polystyrene-block-poly(L-lactide) diblock copolymers, Macromolecules **46**, 2997 (2013).

[19] C. Mille, E. C. Tyrode, and R. W. Corkery, Inorganic chiral 3-D photonic crystals with bicontinuous gyroid structure replicated from butterfly wing scales, Chem. Commun. **47**, 9873 (2011).

[20] S. Vignolini, N. A. Yufa, P. S. Cunha, S. Guldin, I. Rushkin, M. Stefik, K. Hur, U. Wiesner, J. J. Baumberg, and U. Steiner, A 3D optical metamaterial made by self-assembly, Adv. Mater. **24**, OP23 (2012).

[21] X. Cao, D. Xu, Y. Yao, L. Han, O. Terasaki, and S. Che, Interconversion of triply periodic constant mean curvature surface structures: From double diamond to single gyroid, Chem. Mater. **28**, 3691 (2016).

[22] C. Bao, S. Che, and L. Han, Discovery of single gyroid structure in self-assembly of block copolymer with inorganic precursors, J. Hazard. Mater. **402**, 123538 (2021).

[23] P. Chen, M. K. Mahanthappa, and K. D. Dorfman, Stability of cubic single network phases in diblock copolymer melts, J. Polym. Sci. **60**, 2543 (2022).

[24] Q. Xie, Y. Qiang, and W. Li, Single gyroid self-assembled by linear BABAB pentablock copolymer, ACS Macro Lett. **11**, 205 (2022).

[25] H. Park, S. Jo, B. Kang, K. Hur, S. S. Oh, D. Y. Ryu, and S. Lee, Block copolymer gyroids for nanophotonics: Significance of lattice transformations, Nanophotonics **11**, 2583 (2022).

[26] S. S. Oh, A. Demetriadou, S. Wuestner, and O. Hess, On the origin of chirality in nanoplasmonic gyroid metamaterials, Adv. Mater. **25**, 612 (2013).

[27] M. Maldovan, A. M. Urbas, N. Yufa, W. C. Carter, and E. L. Thomas, Photonic properties of bicontinuous cubic microphases, Phys. Rev. B **65**, 165123 (2002).

[28] M. Saba, M. Thiel, M. D. Turner, S. T. Hyde, M. Gu, K. Grosse-Brauckmann, D. N. Neshev, K. Mecke, and G. E. Schröder-Turk, Circular dichroism in biological photonic crystals and cubic chiral nets, Phys. Rev. Lett. **106**, 103902 (2011).

[29] C. Mille, E. C. Tyrode, and R. W. Corkery, 3D titania photonic crystals replicated from gyroid structures in butterfly wing scales: Approaching full band gaps at visible wavelengths, RSC Adv. **3**, 3109 (2013).

[30] S. Peng, R. Zhang, V. H. Chen, E. T. Khabiboulline, P. Braun, and H. A. Atwater, Three-dimensional single gyroid photonic crystals with a mid-infrared bandgap, ACS Photonics **3**, 1131 (2016).

[31] Z. Gan, M. D. Turner, and M. Gu, Biomimetic gyroid nanostructures exceeding their natural origins, Sci. Adv. **2**, e1600084 (2016).

[32] C. K. Ullal, M. Maldovan, E. L. Thomas, G. Chen, Y. J. Han, and S. Yang, Photonic crystals through holographic lithography: Simple cubic, diamond-like, and gyroid-like structures, Appl. Phys. Lett. **84**, 5434 (2004).

[33] C. A. Tyler and D. C. Morse, Orthorhombic *Fddd* network in triblock and diblock copolymer melts, Phys. Rev. Lett. **94**, 208302 (2005).

[34] S. J. Park, F. S. Bates, and K. D. Dorfman, Complex phase behavior in binary blends of AB diblock copolymer and ABC triblock terpolymer, Macromolecules **56**, 1278 (2023).

[35] K.-C. Yang, C.-T. Yao, L.-Y. Huang, J.-C. Tsai, W.-S. Hung, H.-Y. Hsueh, and R.-M. Ho, Single gyroid-structured metallic nanoporous spheres fabricated from double gyroid-forming block copolymers via templated electroless plating, NPG Asia Mater. **11**, 9 (2019).

[36] H. Y. Hsueh, Y. C. Ling, H. F. Wang, L. Y. C. Chien, Y. C. Hung, E. L. Thomas, and R. M. Ho, Shifting networks to achieve subgroup symmetry properties, Adv. Mater. **26**, 3225 (2014).

[37] T. Higashihara, M. Hayashi, and A. Hirao, Synthesis of well-defined star-branched polymers by stepwise iterative methodology using living anionic polymerization, Prog. Polym. Sci. **36**, 323 (2011).

[38] S. Ito, R. Goseki, T. Ishizone, and A. Hirao, Successive synthesis of well-defined multiarmed miktoarm star polymers by iterative methodology using living anionic polymerization, Eur. Polym. J. **49**, 2545 (2013).

[39] F. Hartmann, B. J. Niebuur, M. Koch, T. Kraus, and M. Gallei, Synthesis and microphase separation of dendrimer-like block copolymers by anionic polymerization strategies, Eur. Polym. J. **187**, 111894 (2023).

[40] See Supplemental Material at http://link.aps.org/supplemental/10.1103/PhysRevMaterials.7.105601 for details of SCFT simulation, candidate phase, free energy decomposition and additional data, which includes Refs. [41–43].

[41] A. Ranjan, J. Qin, and D. C. Morse, Linear response and stability of ordered phases of block copolymer melts, Macromolecules **41**, 942 (2008).

[42] A. Arora, D. C. Morse, F. S. Bates, and K. D. Dorfman, Accelerating self-consistent field theory of block polymers in a variable unit cell, J. Chem. Phys. **146**, 244902 (2017).

[43] M. W. Matsen, Fast and accurate SCFT calculations for periodic block-copolymer morphologies using the spectral method with Anderson mixing, Eur. Phys. J. E **30**, 361 (2009).

[44] T. Zografos, Synthesis and rheological properties of branched polylactide, Ph.D. thesis, University of Minnesota, 2023.

[45] C. Li, Q. Dong, and W. Li, Largely tunable asymmetry of phase diagrams of A(AB)n miktoarm star copolymer, Macromolecules **53**, 10907 (2020).

[46] Y. Seo, D. Woo, L. Li, W. Li, and J. K. Kim, Phase behavior of PS-(PS-*b*-P2VP)₃ miktoarm star copolymer, Macromolecules **54**, 7822 (2021).

[47] M. W. Matsen, Self-consistent field theory and its applications, in *Soft Matter, Vol. 1: Polymer Melts and Mixtures*, edited by G. Gompper and M. Schick (Wiley VCH, Weinheim, 2006).

[48] G. H. Fredrickson, *The Equilibrium Theory of Inhomogeneous Polymers* (Oxford University Press, New York, 2006).

[49] A. Arora, J. Qin, D. C. Morse, K. T. Delaney, G. H. Fredrickson, F. S. Bates, and K. D. Dorfman, Broadly accessible self-consistent field theory for block polymer materials discovery, Macromolecules **49**, 4675 (2016).

[50] G. K. Cheong, A. Chawla, D. C. Morse, and K. D. Dorfman, Open-source code for self-consistent field theory calculations of block polymer phase behavior on graphics processing units, Eur. Phys. J. E **43**, 15 (2020).

[51] M. W. Matsen and F. S. Bates, Block copolymer microstructures in the intermediate-segregation regime, J. Chem. Phys. **106**, 2436 (1997).

[52] X. Feng, C. J. Burke, M. Zhuo, H. Guo, K. Yang, A. Reddy, I. Prasad, R. M. Ho, A. Avgeropoulos, G. M. Grason, and E. L. Thomas, Seeing mesoatomic distortions in soft-matter crystals of a double-gyroid block copolymer, Nature (London) **575**, 175 (2019).

[53] M. W. Matsen, Effect of architecture on the phase behavior of AB-type block copolymer melts, Macromolecules **45**, 2161 (2012).

[54] E. W. Cochran, C. J. Garcia-Cervera, and G. H. Fredrickson, Stability of the gyroid phase in diblock copolymers at strong segregation, Macromolecules **39**, 2449 (2006).

[55] C. T. Lai and A. C. Shi, Binary blends of diblock copolymers: An effective route to novel bicontinuous phases, Macromol. Theory Simul. **30**, 2100019 (2021).